Electron. Mater. Lett., Vol. 12, No. 1 (2016), pp. 67-75
DOI: 10.1007/s13391-015-5281-9

Size Effect on Negative Capacitance at Forward Bias in InGaN/GaN Multiple Quantum Well-Based Blue LED

El-Mostafa Bourim and Jeong In Han*

Department of Chemical and Biochemical Engineering, Dongguk University-Seoul, Seoul 100-715, Korea

(received date: 26 June 2015 / accepted date: 20 November 2015 / published date: 10 January 2016)

Size effect of InGaN/GaN multiple quantum well (MQW) blue light emitting diodes (LEDs), on electrical characteristics in forward bias voltage at high injection current in light emission regime, is observed to induce a substantial dispersion in the current density and normalized negative capacitance (NC) (i.e., capacitance per chip area). The correction of normalized NC by considering the LED *p-n* junction series resistance has been found to be independent of chip area size with lateral dimensions ranging from 100 μm × 100 μm to 400 μm × 400 μm. This fact, confirms that the inductive effect which is usually behind the NC apparition is homogeneously and uniformly distributed across the entire device area and hence the dispersive characteristics are not related to local paths.

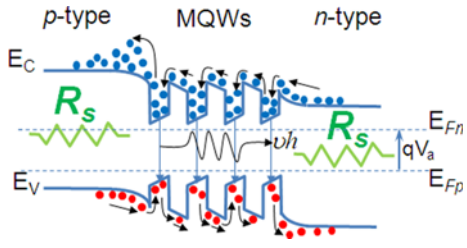

From the characteristics of NC dependence on temperature, frequency and direct current bias, a mechanism based on the electrons/holes charge carriers conductivity difference is proposed to be responsible for the transient electron-hole pair recombination process inducing NC phenomenon. Direct measurement of light emission brightness under modulated frequency demonstrated that modulated light output evolution follows the same behavioral tendency as measured in NC under alternating current signal modulation. Thus it is concluded that the NC is valuable information which would be of practical interest in improving the characteristics and parameters relevant to LED *p-n* junction internal structure.

Keywords: LED, InGaN/GaN, negative capacitance, electron-hole recombination, admittance spectroscopy

1. INTRODUCTION

InGaN/GaN multiple quantum well (MQW)-based light-emitting diodes (LEDs) have been receiving great interest owing to their wide domains of application. Due to their controllable electroluminescence generation LEDs are explored in lighting, color displays, digital displays, major components for solid-state lighting, headlights for automobiles, communicating applications, micro LED display for next generation google glass as well as other electronic and optoelectronic fields.[1-6] In spite of the different progress reached in improving the performance and reliability of LED devices, the physical mechanisms of light emission and electronic transport processes in these materials system are still yet to be analyzed and discussed. The optical and electrical characteristics of LEDs have been the main focus on their performance investigations, while the *ac* (alternating current) characteristics are still sparingly addressed. Such study in the forward *ac* measurements was found to be very important for the LED device physical mechanism comprehension. At large forward bias voltages superposed on *ac* signal, LEDs display negative capacitance (NC). This NC behavior has been observed in many electronic and optoelectronic devices/structures, it is found to take places in Schottky diodes,[7-9] *p-n* junctions,[10] light-emitting diodes,[11-13] solar cells,[14,15] p^+-*i*-n^+ diodes,[16] quantum well infrared photodetectors (QWIPS),[17,18] homojunction far-infrared detectors[19] and inorganic InGaN/GaN MQW based LEDs.[20,21] The microscopic physical mechanisms of the negative capacitance are proposed to be different and have been ascribed mainly to different effects; such as the contact injection,[22] interface states,[23] minority-carrier injections,[24] slow transition time of injected carriers,[22] charge trapping,[12,16]

*Corresponding author: hanji@dongguk.edu

sub-bandgap trap states[25-27] and the like.

Basically the NC phenomenon in semiconductor devices is originating from an inductive effect, which results from the delay of the change in the current flowing in the structure behind the change of the applied bias voltage. Jonscher[28] pointed out that whatever physical origin may be responsible for this phenomenon it must involve temporal evolution of the properties because the negative capacitance is the consequence of a slowly rising current over an interval of time. In the most of cited references above, the NC phenomena are shown to usually occur near the junctions or the interfacial layers, where the conduction mechanisms of inertial conductivity (i.e., current lags behind voltage oscillation) such capture-emission, recombination-generation, and trapping-detrapping take place. For LED devices the inductive effect is believed to take place during the electrons/holes pair (e-h) recombination.[7,11,29] This can be supported by the fact of negative capacitance appearance at the onset of light emission while NC measurements by *ac* admittance system. Thus, this behavior confirms that NC is a proper diode behavior and not an external effect from the measurement system circuits. Furthermore, in LED devices the occurrence of NC has always been associated with forward biased junctions, and the NC dip magnitude is more immersed downward as the modulated frequency is decreased.[21,30-33] In recent papers related to NC in *p-n* junction based LED, the NC was proposed to be due to sub-bandgap trap states (or shallow sates) located in the quantum well (QW) layers, which, under low modulation frequency, participate in charge carrier recombination process at high voltage bias in light emission regime, thus the fast recombination causing light emission compete with slowly responding sub-band defects resulting then in an inductive like behavior.[25]

The aim of this work is to obtain information on the NC behaviors in the LED *p-n* junction diodes, found out the causes from which stem the inductive contribution to the admittance in multi-quantum well based LED, and propose a mechanism explaining the NC origin to gain enhanced insight into the inductive process effect on the LED light emission efficiency. To do so, a comparison of the NC behavior in the InGaN-based μ-LED devices with different emission area sizes ranging from 100×100 to 400×400 μm^2 was investigated. The comparison was made in the characteristics of current density versus voltage (*J-V*), normalized capacitance/conductance versus voltage (*C/G-V*) and normalized capacitance versus frequency (*C-f*). In the *C-f* characteristics, the capacitance was measured under different direct current (*dc*) biases in the light emission regime. We made a correction of the measured capacitance using Nicollian and Brews's model which considers the series resistance of the LED *p-n* junction in the calculation of the capacitance in high current injection regime, and showed that the corrected NC phenomenon is independent of LED size, signifying that the inductive conduction is taking part uniformly and distributed homogenously across the total device area surface, as well as the inductive-type impedance characteristics are governed by the LED series resistance modulation. From the NC characteristic dependence on temperature, frequency and *dc* bias voltage, we proposed a mechanism explaining the origin of negative capacitance and its associated inductive impedance. This mechanism is based on the transient behavior of electron-hole pair recombination in LED quantum wells arising from the difference in charge carrier rate admission and transport into the LED active region. And finally, we measured modulated light output from diode and found a correlation between NC and light emission. The modulated light emission evolution follows the same NC frequency trend behavior, which would make it practical to predict the LED efficiency and performance only from the NC characteristics analysis.

2. EXPERIMENTAL PROCEDURE

The InGaN/GaN-MQW based μ-LED device arrays of different area sizes reported in this paper are made from 450 nm-emitting wafer grown on commercial (0001*) c*-plane sapphire substrate by metal organic chemical vapor deposition (MOCVD) (Aixtron G3 2600). The details of the epitaxial growth conditions are given elsewhere.[6] Following is a sequential description of steps involved in the stack of the different layers constituting the μ-LED device structure: First, on the sapphire substrate was deposited a 30 nm-tick GaN nucleation layer. Followed by the sequential growth of a 2 μm-tick undoped buffer GaN, next a 3 μm-thick Si-doped *n*-type GaN layer with doping concentration of $1 \sim 5 \times 10^{18}/cm^3$. During the growth of the *n*-type GaN layer, a super-lattice structure (SLs) of 10 AlGaN/GaN periods composed of 5.0 nm-thick $Al_{0.2}GaN$ and 10.0 nm-thick GaN (AlGaN/GaN) layers were inserted into the Si-doped *n*-GaN epilayer, with a cap of 400 nm thick *n*-GaN. Next after, 7 periods of 5.0 nm $In_{0.05}Ga_{0.95}N$ and 10.0 nm GaN (InGaN/GaN) pair layers grown to play the role of electron reservoir layers. Then, four pairs of $In_{0.17}Ga_{0.83}N$/GaN MQWs with InGaN well 3.0 nm-thick and GaN barrier 7.0 nm-thick. Finally, a 150 nm thick *p*-GaN with bicyclopentadienyl magnesium (Cp2Mg) dopant with a hole concentration of $4.5 \sim 6.1 \times 10^{17}$ cm^{-3}. After the growth of the epitaxial LED structure, LED chips of different squared sizes (100×100 μm^2, 200×200 μm^2, 300×300 μm^2 and 400×400 μm^2) were tailored in mesa shapes using conventional photolithography and inductively coupled plasma (ICP) dry etching process. ITO (Indium-tin oxide, transparent conductive thin film) was used as current spreading layer deposited on the *p*-GaN LED surfaces and Cr/Au pads were used as *n*- and *p*-type ohmic contact materials. The complete device

structure is shown schematically in the inset of Fig. 1. The electroluminescence (*EL*) measurements were conducted with a light-current-voltage (*L-I-V*) system (LEOS OPI-150—Optel Precision). The *I-V* leakage current measurements were performed by using an HP 4156B semiconductor parameter analyzer. Admittance measurements; *C/G* as a function of the bias voltage and frequency (*f*), were performed using an HP 4284A precision LCR meter. *ac* admittance spectra were recorded for frequencies ranging from 100 Hz to 1 MHz; the *ac* test signal amplitude was fixed at 50 mV. All of the *dc I-V* and admittance measurements were carried out in the dark in a low vacuum chamber. Modulated light emission was measured by using a Topcon BM7 luminance meter with high precision and high measurement speed, and a function generator (Tektronix AFG2021) to supply *ac* modulation frequency superposed on *dc* bias.

3. RESULTS AND DISCUSSIONS

From the *I-V* measurements the current densities of μ-LED chips of different area size are plotted in linear scale in the Fig. 1. As shown, a strong size-dependent behavior is observed in the forward bias at high current injection regime. The smaller the chip area size the higher the current density measured under the same applied bias voltage. Such abnormal behavior of current density dispersion in relation to the area size in high bias voltage region has been already observed in different previous works undertaken in the InGaN/GaN based micro-LED with different area sizes[21,34-36] and was proposed to be related to a high non-uniformity of the current spreading in the larger chip area. Figure 2 shows the electroluminescence spectra measured for the different μ-LED chip area sizes under an injection current of 100 mA.

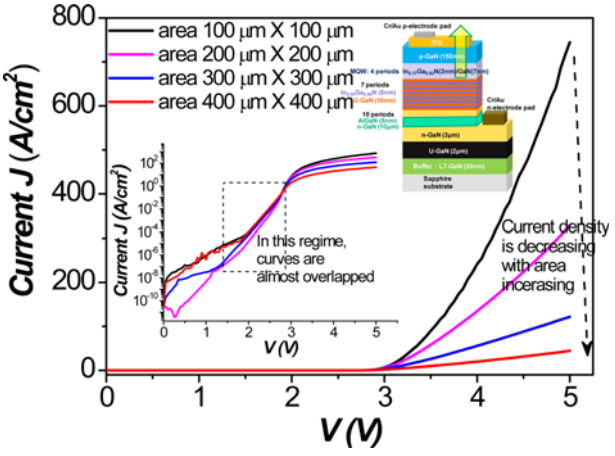

Fig. 1. Characteristics of current density versus voltage bias of μ-LED chips with different area sizes. The left-down inset is the *J-V* plot in semi-logarithmic scale and the right-up inset is a schematic diagram of the LED structure.

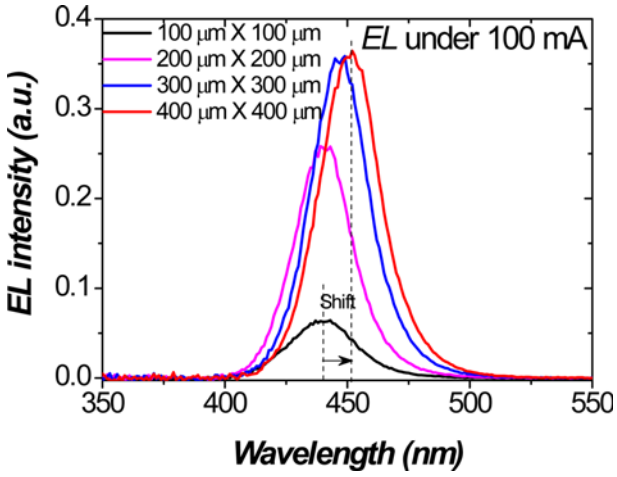

Fig. 2. Electroluminescence spectra of μ-LED chips with different area sizes under a forward injection current of 100 mA.

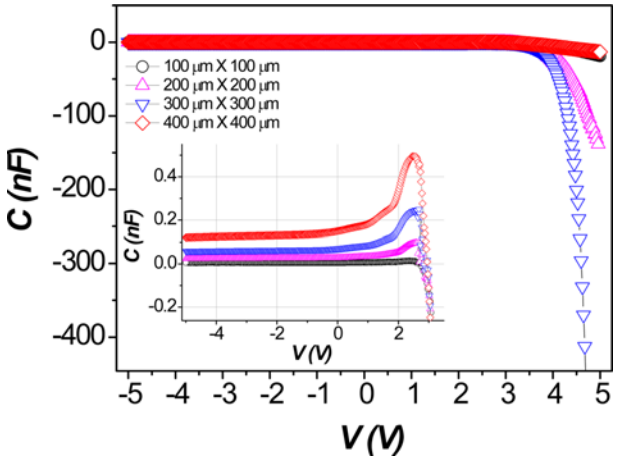

Fig. 3. *C-V* characteristics of μ-LED with different area sizes, the inset shows the capacitance peaks when the capacitance drops toward negative values (The *ac* modulation frequency was fixed at 10 kHz).

The EL intensity increases with μ-LED chip area size and an apparent redshift of the emission wavelength is induced when the chip area size is increased. This wavelength redshift was justified to be associated with the junction self-heating temperature rise with the μ-LED chip area inducing bandgap shrinkage.[35] Figure 3 shows the capacitance-voltage dependence (*C-V*) for different μ-LED chip sizes under an *ac* signal of 10 kHz with applied voltage scan changing from −5 V to +5 V. As is seen in the inset of Fig. 3, the capacitance increases monotonically from negative voltage region to positive voltage region following the Shockley's semiconductor theory, however it undergoes a rapid drop down to negative capacitance values once the applied forward bias goes over turn-on voltage (bias from which the light emission springs up), this behavior is unexpected and is in conflict with the Shockley's theory.

Notice also that the NC magnitude characteristics show a size-dependent behavior except the 400 μm × 400 μm LED chip. Figure 4 shows the capacitance measured at room temperature (RT) with various modulation frequencies for a μ-LED chip of 300 μm × 300 μm area size. The negative capacitance drops to deep negative values as the frequency decreases, as well as when the forward bias voltage increases. Figure 5a shows plots of the capacitance normalized to the chip area (normalized capacitance) as function to the applied bias voltage for the μ-LED chips of different area sizes. It is seen that the curves of normalized capacitance overlap well under low forward bias (inset of Fig. 5a) but deviate to each other at high voltage region where the capacitance is negative. As can also be seen, the normalized NC magnitude value of smaller μ-LED chip area size is higher than that of the larger chip area size under the same large forward bias. Generally, at the high forward bias voltage, during light emission, it has been seen that the normalized NC magnitude decreases as the μ-LED area size is increased. To give an explanation to such abnormal dispersion of normalized NC, an understanding of the NC mechanism and the source from

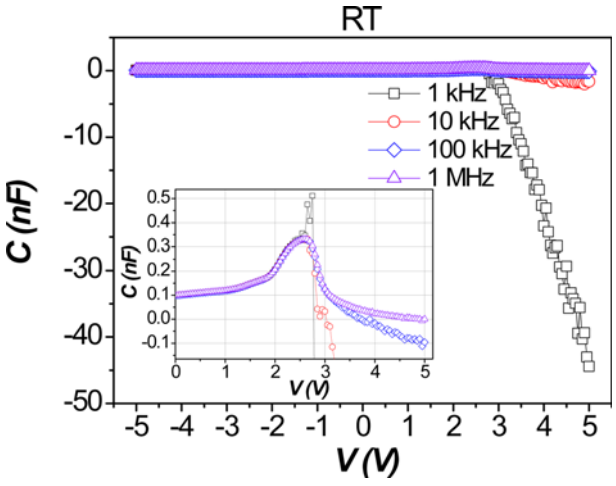

Fig. 4. Frequency-dependent negative capacitance of a μ-LED chip size of 300 μm × 300 μm.

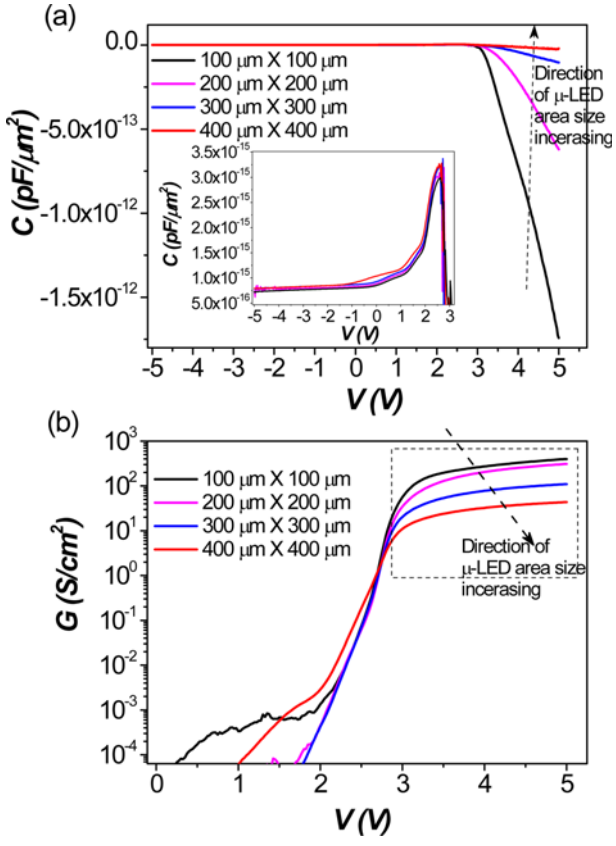

Fig. 5. (a) Characteristics of normalized capacitance under voltage scan from reverse to forward bias of μ-LED chips of different area sizes; (b) Characteristics of normalized conductance of the same chips at medium and high forward bias regimes. (The *ac* modulation frequency was fixed at 10 kHz).

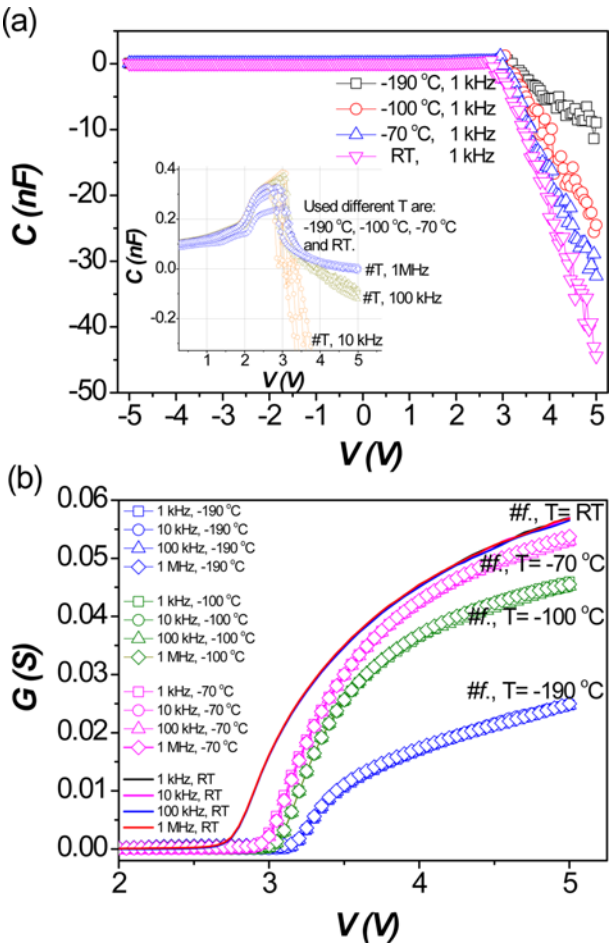

Fig. 6. (a) Temperature-dependent negative capacitance of a μ-LED chip size of 300 μm × 300 μm measured under an *ac* signal of 1 kHz, the inset shows the temperature independence of negative capacitance at higher *ac* signals of 10 kHz, 100 kHz and 1 MHz; (b) *G-V* characteristics of the same chip measured at different temperatures with different *ac* signal frequencies (*#f.*).

which is stemmed is requested. Nevertheless, the effect of size dependent self-heating, by which the junction temperature of a larger μ-LED chip size is higher than that of smaller μ-LED chip size under the same current densities,[35,37] would result in different charge escapes from MQW and hence the normalized NC properties would be dependent on the chip size. Note that the normalized conductance (conductance per chip area) versus bias voltage (Fig. 5b) at medium and high forward bias regions showed the same behavior trend as the current density and the normalized capacitance, an overlapping of the conductance curves at medium bias and a conspicuous dispersion at high voltage region. In order to check the effect of temperature on the NC behavior, Fig. 6a shows the *C-V* characteristics of a 300 μm × 300 μm chip device with temperature changing from −190°C to RT. It is clearly seen that the NC magnitude undergoes a noticeable increase as the temperature increases, a similar trend was observed in other μ-LED chip sizes as well. However, this NC temperature dependence was observed to take place only at low *ac* signal frequency <10 kHz, while for higher frequencies the NC magnitude was found to be less influenced by the temperature variation (see inset of Fig. 6a). On the contrary, the conductance, *G*, measured in the voltage region where the NC takes place, showed practically no dependence on the *ac* frequency modulation whatever the frequency range, but a significant *G*-dependence on the ambient temperatures was observed (see Fig. 6b).

To study the effect of modulation frequency and *dc* bias amplitude on the negative capacitance for the μ-LED chips of different area sizes, Fig. 7 shows a set of measurements of the variation of absolute normalized capacitance versus frequency modulation for different chip area sizes under different *dc* forward biases of +3.25 V, +4 V and +5 V corresponding to light emission regime. For the sake of clarity, the capacitance is represented by its absolute value in logarithmic scale in which the NC magnitude region is indicated by symbol (−C) while the normal positive capacitance by symbol (+C). The transition between these two capacitance modes is identified with a spike like shape. As seen for the different chip area sizes and applied *dc* biases, the normalized log|NC| is obvious a low frequency and decreases almost linearly as the frequency increases, then after the transition (−C to +C) the normalized capacitance magnitude evolves in plateau shape-like, as can be seen almost independently of the chip area sizes. In addition to the normalized NC magnitude dependence on the chip size and *dc* bias strength as has already been seen in *C-V* measurements, it is relevant to point out that the spike frequency was found to be, both, LED chip area size and *dc* bias dependent as well. The spike frequency moves to higher values when increasing either the chip area size or the *dc* bias. Furthermore, it is worth to note that the NC magnitude dependence on frequency could be expressed as a power law

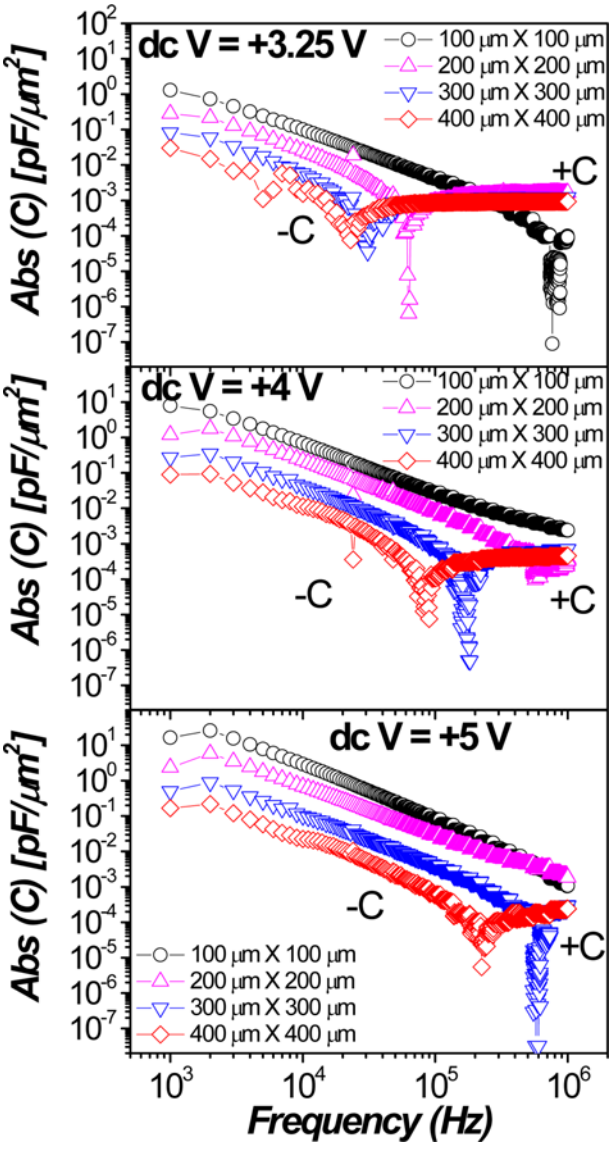

Fig. 7. Absolute normalized capacitance versus frequency recorded under different *dc* bias voltages for μ-LED chips of different area sizes.

function of frequency as has already been found in other studies.[28,32]

Since the NC effect is shown to take place specifically at high current injection regime in forward voltage region where series resistance could have an imminent effect on the inductive conduction. In fact, a part from the total charge carriers injected for being recombined in the QW region could diffuse to the *n*- and *p*-type quasi-neutral semiconductor regions as minority carriers. These carriers can modulate the series resistances (R_s) of *p-n* semiconductor materials;[9,38,39] and hence the R_s change would have a palpable influence on the measured admittance as well as the charge transport controlling the inductive effect. From this point of view an extraction of the R_s effect on the NC would shed light to

understand the mechanisms underlying the NC effect.

Given that in our investigated LED structure the doping density in the *n*-type region considerably exceeds the doping of doped *p*-type region, we can without substantial inaccuracy state that the *p*-*n* junction space charge region (SCR) completely spreads to the lightly doped *p*-type base,[40-43] and hence the narrowed *n*-type base would be considered as part of the metallic contact. Such structure can be assimilated to a metal-insulator-semiconductor (MIS) Schottky diode for which according to the model presented by Nicollian and Brews,[44] the real R_s can be determined from the measured capacitance (C_m) and the conductance (G_m) in the strong accumulation regime. Therefore the measured capacitance and conductance can be corrected by considering the R_s effects to obtain the real capacitance and conductance values (C_c and G_c). We can extract corrected admittance components using the following relations:

$$C_c = \frac{(G_m^2+(\omega C_m)^2)C_m}{a^2+(\omega C_m)^2} \text{ and } G_c = \frac{(G_m^2+(\omega C_m)^2)a}{a^2+(\omega C_m)^2} \quad (1)$$

where a and R_s are given in the following forms:

$$a = C_m - [G_m^2+(\omega C_m)^2]R_S \quad (2)$$

$$R_S = \frac{G_m}{G_m^2+(\omega C_m)^2} \quad (3)$$

Figure 8 depict the corrected normalized capacitance characteristics of μ-LED device with different area sizes as a function of frequency for *dc* bias voltages of +3.25 V, +4 V and +5 V at room temperature. In the all frequency range the normalized capacitance magnitude underwent a perceivable diminution after the correction, however it is clearly seen that the corrected capacitances C_c in the inductive regime corresponding to NC do show no more size effect dependence for the different μ-LED chip areas. For the all three applied *dc* bias voltages the corrected NC in the inductive regime is still showing the same power law trend as before the correction; which manifested in a decrease of the normalized log|NC| with frequency increase until the transition to capacitive regime. In this later regime the normalized capacitance corrections (C_c) are manifested in a large dispersion and their magnitude levels are shown to increase as the LED chip area increases. At present we do not have any conclusive explanation to justify such behavior. Nevertheless, the non dependence of the normalized NC_c on the chip area size means that the inductive conduction is homogenous and uniformly distributed through the whole QW layers where is taking place, as well as similar for all μ-LED device area sizes. Therefore, the normalized NC dispersion that was seen in low frequency range without considering the R_s effect could be justified by the LED *p*-*n* junction self-heating temperature which is higher for the

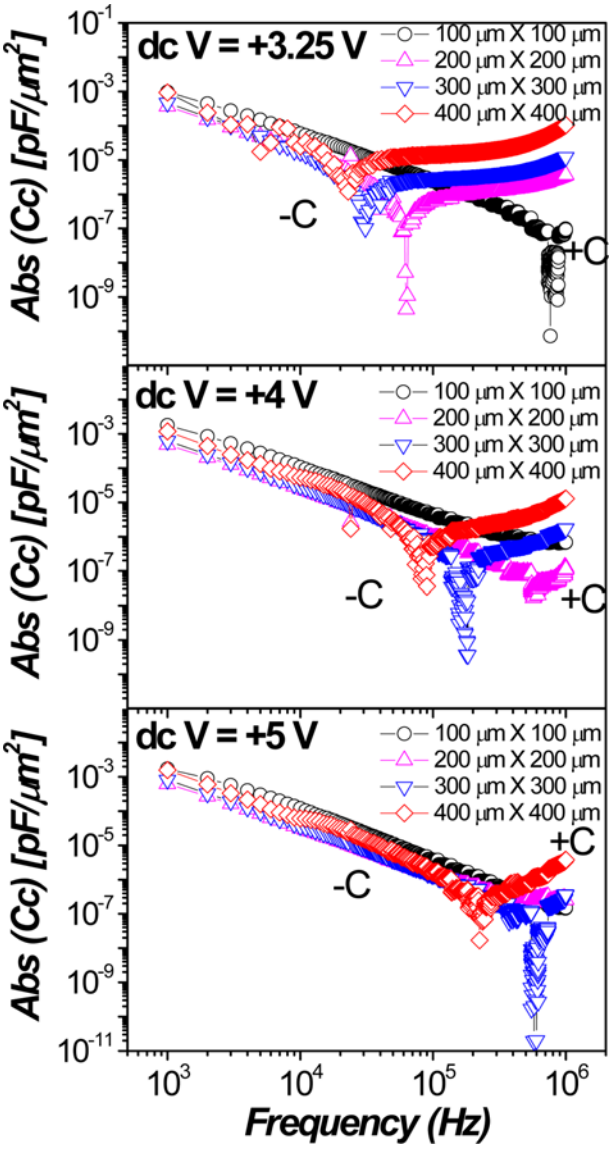

Fig. 8. Absolute corrected normalized capacitance versus frequency recorded under different *dc* bias voltages for μ-LED chips of different area sizes.

injected current in large area LED device and can generate an escape of charge carriers from QWs to the semiconductor quasi-neutral regions.[25-27] Such charge carrier escape causes two simultaneous change in the electrical characteristics: 1) reduces the charge participation in the e-h recombination, this can be detected during the inductive conduction regime by a significant decrease in the NC magnitude for μ-LEDs with large area size, 2) enhances R_s by the escaped carriers from MQW considered as minority carriers injected in the semiconductor quasi-neutral region (see Fig. 9a). As a matter of fact, it would be acceptable to consider that the augmentation of R_s is responsible for the low leakage current density measured in large area μ-LED as seen in *J*-*V* in Fig.

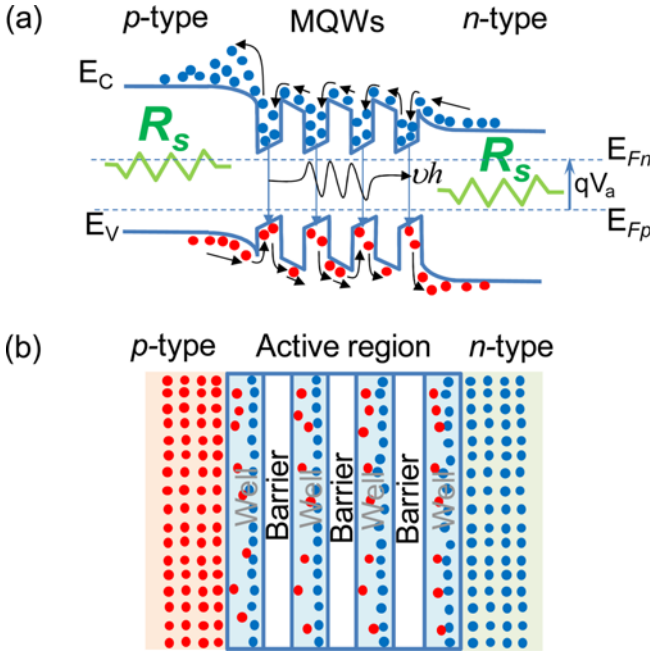

Fig. 9. (a) Energy band diagram configuration at high forward regime showing R_s modulations by charge escape from QWs to quasi-neutral regions of *p-n* junction semiconductors, (b) Scheme configuring the inductive conduction scenario by the presence of electron and hole in different amount in the well layers due to the difference of charge carrier mobility. The blue and red solid circles denote electrons and holes, respectively, and the arrows indicate the directions of charge-carriers motion.

1. However the low frequency shown in the transition from the inductive to capacitive behavior for the large area μ-LED chip is related to its total chip resistance which is the smallest compared to the resistance of other small μ-LED chip sizes. Hence, according to the current relaxation for a transient inductive circuit ($\tau = L/R$), the relaxation time domain, in transiting from inductive to capacitive mode for LED chip with small resistance, will be larger than the one with high resistance. This justifies the short inductive frequency domain range associated to the large area LED (having low resistance) and the wide inductive frequency domain range associated to the small area LED (having higher resistance). Based on these data describing the capacitance dependence on frequency and *dc* bias, the NC characteristics (magnitude and transition frequency) are seeing to be directly connected to *dc* bias amplitude, and the log|*NC*| vs log(*f*) plots for different *dc* biases show parallel slopes, which means that the inductive phenomenon controlling the e-h recombination rate is solely frequency dependent. So what could be the origin of the mechanism of the inductive like behavior?

Bansal *et al*. in their recent works on NC in AlGaInP based MQW LED have proposed that the inductive effect is related to the recombination current flow controlled by the sub-bandgap defect interaction with QW's charge carriers.[25] However, in our previous study, on the InGaN/GaN based LED device (similar to the ones investigated in this paper) by admittance spectroscopy in low and high temperatures for *dc* bias amplitudes lower than LED turn-on voltage,[6] no signal related neither to interface states nor bulk defects was detected. Furthermore, the temperature dependent NC signal was revealed to be significantly active only in probing frequency range lower than tens of kilo-hertz (Fig. 6), while the temperature effect on the response of defect states located either in bulk or interface of crystal semiconductors with medium band-gap energy can be detected up to an order of mega-hertzs.[45] Based on the above experimental results and analyses, and considering that the current flowing through the LED *p-n* junction in light emission regime is predominantly related to the electron/hole recombination in the MQW regions, one suggests that the inductive like-current flow would be basically due to the charge carrier mobility difference between electrons and holes through the QW barriers in the active region. As commonly known, electrons have generally higher mobility than holes, thus the fast injected electrons admitted in the QW's conduction band (causing high amount of electron presence in the well layers) will recombine with slow admitted holes in the QW's valence band (causing small amount of hole presence in the well layers) (Fig. 9b) in a way leading to an inductive conduction process stemmed from the e-h recombination rate dependence on the hole response time. This mechanism is well supported by the frequency dependence of the minority carrier's responses in *n* and *p*-type Metal-Oxide-Semiconductor MOS structures when biased in the inverse regime. Under the electric field, the hole carrier response in MOS(*n*) structure by capacitance measurements was found to be revealed only in the quasi-static frequency regimes, while electron carrier response in MOS(*p*) structure was revealed even up to MHz range.[46]

To check the correspondence in behavior between the NC and the light emission, a direct light output brightness measurement as function of modulated frequency was performed. Figure 10 shows modulated light output brightness frequency dependence for a μ-LED device with an area size of 400 μm × 400 μm under a *dc* bias of +4 V and *ac* signal of 100 mV. As can be seen, in the low frequency range the modulated light output brightness magnitude decreases as the modulation frequency is increased following a power law tendency, then stabilizes after reaching higher modulation frequency range (over tens of kHz). Such behavior coincides well with capacitance spectrum evolution in light emission regime (Fig. 7); where the frequency dependent NC part (-C) corresponds to the modulated light output brightness magnitude variation with frequency and the quasi-stable positive capacitance part (+C) corresponds to the quasi-stabilized light output brightness becoming independent of the modulation frequency. The correlation between the NC

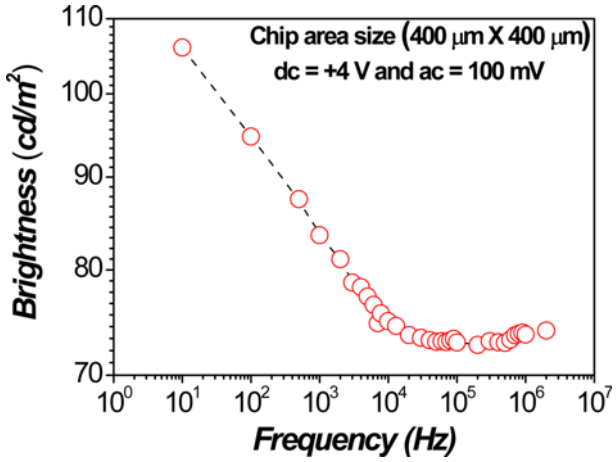

Fig. 10. Light output brightness modulated with an *ac* signal superposed to a *dc* bias of 4 V for a μ-LED chip of 400 μm × 400 μm area size.

and the modulated light output evolutions proves that the inductive phenomenon generated in the LED *p-n* junction has a direct effect on the charge carrier recombination in the active MQW region. Accordingly, the model based on the transient behavior in the rate variation of electron-hole pair recombination arising from the difference in charge carrier (electrons and holes) transport in the LED MQW active region could be a potential mechanism, which needs to be investigated in details in future works by checking the hole response time effect on the e-h recombination rate either by changing the *p*-type region conductivity with doping or by inserting a hole supplier layer in the LED structure. Furthermore, the evident correlation observed in the correspondence between the NC and the modulated light emission behavior processes under frequency modulation effect, demonstrates that the LED efficiency and performance could be practically investigated only from the NC characteristics analysis.

4. CONCLUSIONS

In this paper, we have investigated the negative capacitance behavior through μ-LED size effect on the electrical and optical characteristics performed on InGaN/GaN MQW LEDs with size ranging from 100 μm × 100 μm to 400 μm × 400 μm. Under high forward bias voltages in the light emission regime, the observed anomalous dispersion of current density and normalized NC for μ-LED of different size was suggested to be influenced by self-heating temperature resulting in thermal escape of charge carriers from QWs active region. Hence, the charge carrier escape has twofold: 1) increasing the *p-n* junction series resistance by the fact that the injected carriers are minority carriers modulating the conductivity of the LED *p-n* junction semiconductor quasi-neutral regions which results in a low leakage current as the μ-LED area increases, 2) reducing the e-h recombination intensity which leads to a decrease in the NC signal with the increase of μ-LED area. Correction of the measured NC by considering the series resistance influence in the admittance response at high current injection demonstrated that the normalized NC is independent of the μ-LED area size and that the inductive process, from which the NC is stemmed, is uniformly and homogeneously distributed through the whole μ-LED device area. Accordingly, this confirms no existence of local conduction paths in the investigated μ-LED chips and the observed dispersive behaviors in the current density and normalized NC were related to self-heating temperature influence. From the analysis of the electrical and optical characteristics measured on μ-LED of different sizes, a mechanism explaining the origin of the inductive process emergence in the LED *p-n* junction is proposed to be due to a monotonic e-h recombination rate variation, generated by mobility difference of charge carriers (electrons/holes) through the MQW-LED device active region layers. Furthermore, the observed correlation between the modulated light output and the frequency dependent NC demonstrates that admittance characteristics under high forward bias would be of practical interest for evaluating the LED efficiency and performance only from the NC characteristics analysis.

ACKNOWLEDGMENTS

This work was supported by the Civil-Military Technology Cooperation Center (13-DU-EE-13). The authors would like to thank Dr. H.C. Moon and Mr. H.D. Moon of EyeD Ind. Company (Suwon, South Korea) for the supply of the micro-LED samples used in this study.

REFERENCES

1. H. Morkoc, *Handbook of Nitride Semiconductors and Devices, Vol. 3*, *GaN-based Optical and Electronic Devices,* WILEY-VCH Verlag GmbH & Co. KGaA, Weinheim (2009).
2. F. A. Ponce and D. P. Bour, *Nature* **386**, 351 (1997).
3. I. Akasaki, *Proc. IEEE* **101**, 10, 2200 (2013).
4. Z. Y. Fan, J. Y. Lin, and H. X. Jiang, *J. Phys. D: Appl. Phys.* **41**, 094001 (2008).
5. S. Lee, G. Yoo, J. Jang, Y. Won, and O. Nam, *Electron. Mater. Lett*. **10**, 67 (2014).
6. E.-M. Bourim, and J. I. Han, *Electron. Mater. Lett*. **11**, 982 (2015).
7. F. Sandoval, C. Lopez, and E. Munoz, *Solid-State Electron.* **25**, 355 (1982).
8. X. Wu, E. S. Yang, and H. L. Evans, *J. Appl. Phys.* **68**, 2845 (1990).
9. C. H. Champmess and W. R. Clark, *Appl. Phys. Lett.* **56**, 1104 (1990).

10. T. Noguchi, M. Kitagawa, and I. Taniguchio, *Jpn. J. Appl. Phys.* **19**, 1423 (1980).
11. C. Y. Zhu, L. F. Feng, C. D. Wang, H. X. Cong, G. Y. Zhang, Z. J. Yang, and Z. Z. Chen, *Solid State Electron.* **53**, 324 (2009).
12. L. S. C. Pingree, B. J. Scott, M. T. Russell, T. J. Marks, and M. C. Hersam, *Appl. Phys. Lett*. **86**, 073509-1 (2005).
13. J. Bisquert, G. Garcia-Belmonte, A. Pitarch, and H. J. Bolink, *Chem. Phys. Lett.* **422**, 184 (2006).
14. H. H. P. Gommans, M. Kemerink, and R. A. J. Janssen, *Phys. Rev. B* **72**, 235204-1 (2005).
15. I. Mora-Seró, J. Bisquert, F. Fabregat-Santiago, G. Garcia-Belmonte, G. Zoppi, K. Durose, Y. Proskuryakov, I. Oja, A. Belaidi, T. Dittrich, R. Tena-Zaera, A. Katty, C. Lévy-Clément, V. Barrioz, and S. J. C. Irvine, *Nano Lett.* **6**, 640 (2006).
16. F. Lemmi and N. M. Johnson, *Appl. Phys. Lett.* **74**, 251 (1999).
17. H. C. Liu, Z.R. Wasilewski, M. Buchanan, and H. Chu, *Appl. Phys. Lett.* **63**, 761 (1993).
18. M. Ershov, H. C. Liu, L. Li, M. Buchanan, Z. R. Wasilewski, and V. Ryzhii, *Appl. Phys. Lett*. **70**, 1828 (1997).
19. A. G. U. Perera, W. Z. Shen, and M. E. Shov, *Appl. Phys. Lett.* **74**, 3167-9 (1999).
20. W. Yang, D. Li, J. He, C. Wang, and X. Hu, *Phys. Status Solidi C* **11**, 714 (2014).
21. W. Yang, S. Zhang, J. J. D. McKendry, J. Herrnsdorf, P. Tian, Z. Gong, Q. Ji, I. M. Watson, E. Gu, M. D. Dawson, L. Feng, C. Wang, and X. Hu, *J. Appl. Phys*. **116**, 044512 (2014).
22. M. Ershov, H. C. Liu, L. Li, M. Buchanan, Z. R. Wasilewski, and A. K. Jonscher, *IEEE Trans. Electron. Dev.* **45**, 2196 (1998).
23. X. Wu, E. S. Yang, and H. L. Evans, *J. Appl. Phys.* **68**, 2845 (1990).
24. C. H. Champness and W. R. Clark, *Appl. Phys. Lett.* **56**, 1104 (1990).
25. K. Bansal and S. Datta, *J. Appl. Phys.* **110**, 114509 (2011).
26. K. Bansal and S. Datta, *Appl. Phys. Lett.* **102**, 053508 (2013).
27. K. Bansal and S. Datta, *Mater. Res. Soc. Symp. Proc.* **1635**, 49 (2014).
28. A. K. Jonscher, *J. Chem. Soc., Faraday Trans.* **2**, 75 (1986).
29. E. Ehrenfreund, C. Lungenschmied, G. Dennler, H. Neugebauer, and N. S. Sariciftci, *Appl. Phys. Lett.* **91**, 012112 (2007).
30. C. Y. Zhu, L. F. Feng, C. D. Wang, H. X. Cong, G. Y. Zhang, Z. J. Yang, and Z. Z. Chen, *Solid-State Electron*. **53**, 324 (2009).
31. L. F. Feng, J. Wang, C. Y. Zhu, H. X. Cong, Y. Chen, and C. D. Wang, *Optoelectron. Lett.* **1**, 0124 (2005).
32. Y. Li, C. D. Wang, L. F. Feng, C. Y. Zhu, H. X. Cong, D. Li, and G. Y. Zhang, *J. Appl. Phys.* **109**, 124506 (2011).
33. Y. Li, L. F. Feng, Q. Y. Xing, and X. L. Wang, *J. Electr. Mater.* **44**, 3, 999 (2015).
34. S. X. Jin, J. Shakya, J. Y. Lin, and H. X. Jiang, *Appl. Phys. Lett*. **78**, 3532 (2001).
35. Z. Gong, S. Jin, Y. Chen, J. McKendry, D. Massoubre, I. M. Watson, E. Gu, and M. D. Dawson, *J. Appl. Phys.* **107**, 013103 (2010).
36. P. Tian, J. J. D. McKendry, Z. Gong, B. Guilhabert, I. M. Watson, E. Gu, Z. Chen, G. Zhang, and M. D. Dawson, *Appl. Phys. Lett.* **101**, 231110 (2012).
37. T.-I. Kim, Y. H. Jung, J. Song, D. Kim, Y. Li, H.-S. Kim, I.-S. Song, J. J. Wierer, H. A. Pao, Y. Huang, and J. A. Rogers, *Small* **8**, 1643 (2012).
38. J. Werner, A. F. J. Levi, R. T. Tung, M. Anzlowar, and M. Pinto, *Phys. Rev. Lett.* **60**, 53 (1988).
39. M. A. Green and J. Shewchun, *Solid-Slate Electron*. **16**, 1141 (1973).
40. Y. Zohta, Hi. Kuroda, R. Nii, and S. Nakamura, *J. Cryst. Growth* **189-190**, 816 (1998).
41. N. D. Nguyen, M. Schmeits, M. Germain, B. Schineller, and M. Heuken, *Phys. Stat. Sol. (c)* **0**, 1, 288 (2002).
42. A. Y. Polyakov, A. V. Govorkov, N. B. Smirnov, A. V. Markov, I.-H. Lee, J.-W. Ju, S. Yu. Karpov, N. M. Shmidt, and S. J. Pearton, *J. Appl. Phys* .**105**, 123708-1 (2009).
43. O. V. Kucherovaa, V. I. Zubkova, A. V. Solomonova, and D. V. Davydov, *Semiconductors* **44**, 335 (2010).
44. E. H. Nicollian and J. R. Brews, *Metal Oxide Semiconductor (MOS) Physics and Technology*, Wiley, N. Y. (1982).
45. S. M. Sze, *Physics of Semiconductor Devices*, 2nd ed., J. Wiley & Sons, N. Y. (1981).
46. S.-J. Chang and J.-G. Hwu, *IEEE Tran. Electr. Dev.* **58**, 684 (2011).